MagX: Wearable, Untethered Hands Tracking with Passive Magnets

Dongyao Chen[+], Mingke Wang[+], Chenxi He[+], Qing Luo[+],
Yasha Iravantchi[◇], Alanson Sample[◇], Kang G. Shin[◇], Xinbing Wang[+]
[+] Shanghai Jiao Tong University
{chendy,wangmingke,danielhe2000,luoqing,xwang8}@sjtu.edu.cn
[◇] University of Michigan, Ann Arbor
{yiravan,apsample,kgshin}@umich.edu

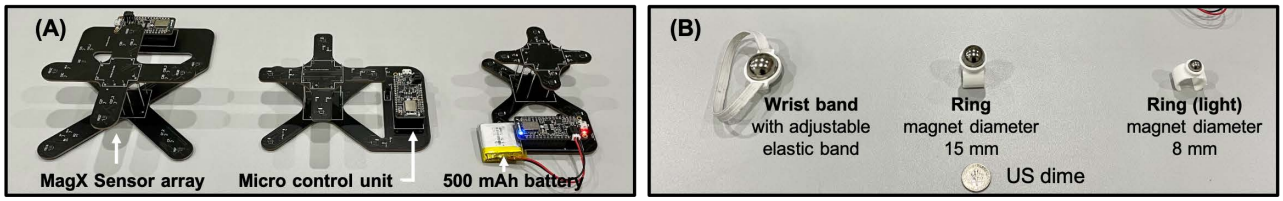

Figure 1: MagX provides a wearable and untethered sensing module, with customizable array sizes and versatile form factors by using passive magnets. (A) MagX with three different sensor array sizes; (B) three form factors with different magnet configurations. Both images are on the same scale.

ABSTRACT

Accurate tracking of the hands and fingers allows users to employ natural gestures in various interactive applications. Hand tracking also supports health applications, such as monitoring face-touching, a common vector for infectious disease. However, for both types of applications, the utility of hand tracking is often limited by the impracticality of bulky tethered systems (e.g., instrumented gloves) or inherent limitations (e.g., Line of Sight or privacy concerns with vision-based systems). These limitations have severely restricted the adoption of hand tracking in real-world applications. We present MagX, a fully untethered on-body hand tracking system utilizing passive magnets and a novel magnetic sensing platform. Since passive magnets require no maintenance, they can be worn on the hands indefinitely, and only the sensor board needs recharging, akin to a smartwatch.

We used MagX to conduct a series of experiments, finding a wearable sensing array can achieve *millimeter-accurate* 5 DoF tracking of two magnets independently. For example, at 11 cm distance, a $6cm \times 6cm$ sensing array can achieve positional and orientational errors of 0.76 cm and 0.11 rad. At 21 cm distance, the tracking errors are 2.65 cm and 0.41 rad. MagX can leverage larger sensor arrays for improved long-distance tracking, e.g., a $9.8cm \times 9.8cm$ array can achieve 2.62 cm and 0.55 rad tracking performance on two magnets at 27 cm distance. The robust performance can facilitate ubiquitous adoption of magnetic tracking in various applications. Finally, MagX can perform all compute locally and only requires 0.38W total ($220mW$ on the sensor platform plus $159mW$ on the computing unit) to perform real-time tracking, offering "all day" fully untethered operation on a typical smartwatch-sized battery.

ACM MobiCom '21, October 25–29, 2021, New Orleans, LA, USA

ACM ISBN 978-1-4503-8342-4/21/10…$15.00
https://doi.org/10.1145/3447993.3483260

CCS CONCEPTS

• **Human-centered computing → Ubiquitous and mobile computing systems and tools**.

KEYWORDS

Hand Tracking, Magnetic Sensing, Untethered

ACM Reference Format:
Dongyao Chen[+], Mingke Wang[+], Chenxi He[+], Qing Luo[+],, Yasha Iravantchi[◇], Alanson Sample[◇], Kang G. Shin[◇], Xinbing Wang[+]. 2021. MagX: Wearable, Untethered Hands Tracking with Passive Magnets. In *The 27th Annual International Conference on Mobile Computing and Networking (ACM MobiCom '21), October 25–29, 2021, New Orleans, LA, USA.* ACM, New York, NY, USA, 14 pages. https://doi.org/10.1145/3447993.3483260

1 INTRODUCTION

As one of the most expressive parts of the body, the hands offer a natural way to interact with machines and the surrounding environment. Precise hand tracking technology helps boost user experience by improving the immersion of the interaction, which is critical to VR/AR environments. Furthermore, hand gestures are usually relevant to mental stress (e.g., subconscious hair pulling, lip picking, fingernail chewing) and physical well-being (hand-washing and face-touching), especially in the COVID-19 pandemic era.

Many prior studies have gravitated towards using cameras and/or Inertial Measurement Units (IMUs) as sensors to track users' hands. As the most prevailing solution for hand tracking, the camera-based approaches have enabled high-precision hand segmentation and

tracking. However, the line-of-sight (LoS) requirement, high energy/computation costs, and privacy concerns hamper the adoption of these methods for mobile applications. IMUs offer a solution to these issues. Specifically, they can be placed in any strategic location on the human body to allow direct query of the state of the deployed position. They are not reliant on LoS and do not pose a privacy issue in the same manner as cameras. However, their fundamental limitation is the drifting problem, where the estimated position accumulates tracking error over time. Furthermore, fine-grained hand pose tracking requires multiple IMUs on the hand. Running all units simultaneously and continuously makes it too power-hungry to support all-day usage on a smartwatch-sized battery. These listed issues ultimately limit the feasibility of these approaches in the real world.

We present MagX, a fully *wearable* and *untethered* on-body hand tracking system utilizing passive magnets and a novel magnetic sensing platform. The nature of magnetic fields allows for LoS resilient and privacy-preserving sensing. Since fixed magnets require no maintenance, they can be worn on hands indefinitely, and only the sensor board needs recharging, akin to a smartwatch. To build MagX, we focus on achieving three fundamental features:

- **Robust.** The tracking performance needs to be robust against fast-changing environmental noise and various hand poses;
- **High-efficiency.** MagX should employ energy-efficient sensing and computational approaches to perform fully integrated on-body sensing;
- **Low-cost & wearability.** MagX should have low manufacturing cost and high wearability.

Achieving robust magnetic tracking is challenging due to the speed and variety of hand movements and varying environmental magnetic noise. Specifically, a hand-worn magnet's orientation (i.e., the magnetic pole) may change quickly, inducing a highly-dynamic spatial distribution of the magnetic flux density. Different environments introduce unique background magnetic field conditions, including Earth's magnetic field and hard/soft iron effects from nearby metallic objects. Therefore, the magnetic field of the targeted magnets can easily be overpowered by the aforementioned noises, rendering wearable passive magnet tracking a challenging task. To tackle this problem, we track the 5 DoF information of magnet(s) by using the Levenberg–Marquardt (LM) algorithm. The LM-based method derives two types of essential information: the targeted magnet's status (i.e., spatial, angular, and magnet moment) and the background magnetic field. This enriched awareness of the background information allows MagX to *decouple* system noise from environmental changes, thus improving the system's robustness.

Building a fully-integrated wearable magnetic tracking platform presents additional challenges as existing approaches usually employ (1) a bulky frontend for collecting magnetic field data, and (2) a tethered backend (e.g., a laptop) to provide unbounded computational resources. In contrast, MagX is a fully wearable and untethered system, with a novel magnetometer sensor array design pipeline aided by simulation and Particle Swam Optimization (PSO) algorithm. To validate the real-world performance of the designed platform, we propose a new benchmarking tool that leverages a commodity off-the-shelf (COTS) LeapMotion infrared camera. Compared to expensive, conventional motion capture (MoCap) systems, our platform is low-cost and easy-to-use without compromising accuracy. We streamline the above design steps into a computer-aided magnetometer array design (CAMAD) pipeline, which will be detailed in Sec. 4.

To further improve the efficiency of MagX, we conduct in-depth code optimization of the tracking algorithm, achieving 5 DoF tracking on mobile platforms, e.g., Raspberry Pi 4B. Our experimental results indicate MagX is able to accurately track multiple magnets in real-time. Specifically, a $6cm \times 6cm$ (of the XY-plane) sensing array can achieve positional and orientational errors of 0.93 cm and 0.09 rad on one magnet; 0.76 cm and 0.11 rad on two magnets, at 11 cm distance. Using the same array, MagX retains robust tracking at longer distances: 2.22 cm and 0.16 rad on one magnet and 2.65 cm and 0.41 rad on two magnets at 21 cm away. MagX can leverage larger arrays for improved long-distance tracking: a $9.8cm \times 9.8cm$ array can achieve positional and orientational errors of 0.51 cm and 0.04 rad on one magnet; 0.46 cm and 0.10 rad on two magnets, at 11 cm. At 27 cm distance, the same array can achieve 1.36 cm and 0.14 rad on one magnet; 2.62 cm and 0.55 rad on two magnets.

MagX is also highly wearable with low energy consumption. Results show that real-time data collection and tracking incur extra power drain $0.65W$ on a Raspberry Pi 4B or $0.15W$ on an emulated Raspberry Pi Zero, plus $0.22W$ power consumption of the sensor array itself. Compared to the energy drain of other power-hungry hand tracking systems, MagX's low energy consumption enables its "all day" operation on off-the-shelf smartwatch-sized batteries. See Sec. 5 for Detailed results.

MagX's mobile and untethered feature can enable a wide range of real-world applications. This paper focuses on the evaluation of MagX's usability in three key applications, i.e., subconscious behavior monitoring, enriched user interaction, and at-home healthcare. Specifically, we present and evaluate three representative applications, including face touching detection, controller-free AR interaction, and usage in precision medicine such as endocapsule tracking. These applications will be elaborated in Sec. 6.

To promote further research & development for these applications (e.g., face touching detection for improving personal hygiene in the pandemic era), we have made all source files (e.g., code and Gerber file) of MagX publicly available at https://github.com/dychen24/magx. This paper makes the following contributions:

(1) Introduction of MagX, the first wearable, untethered hands tracking platform based on passive magnets;
(2) A computer-assisted magnetometer array design pipeline for fast prototyping of magnetic tracking hardware;
(3) A series of experimental studies to demonstrate the wearability and usability of MagX in real-world settings;
(4) A comprehensive study of potential real-world applications enabled by MagX.

2 RELATED WORK

We first contextualize MagX relative to general hand tracking approaches. Specifically, we include both gesture-detection approaches (which can track hands' activity but not their position) and more fine-grained pose-estimation approaches (which can track the location of key points on the hands). MagX is situated closer to the latter approach. We then examine existing magnetic tracking works,

including inventions using electromagnets, passive magnets. For reference, MagX leverages multiple passive magnets.

2.1 Hand Tracking Applications

Motion-based. The convenience and ubiquity of IMUs in smartwatches have led to their extensive use in hand and arm tracking. The first class of applications is gesture applications, where a specific hand-based action is classified. More recent work proposes a smartwatch-based system for detecting 25 hand activities and provides a thorough survey of IMU-based hand gesture detection [21]. In light of the recent COVID-19 crisis, face touching has become a particularly pertinent hand gesture for detection and prevention. For example, ImmuTouch [9] leverages the IMU sensors to detect face touching events. Its functionality demands a customized electronic wrist band and a training phase. Similarly, Jalapeno [10] is a Fitbit-based app for face touching detection.

A more challenging class of applications is position-estimation applications, where the precise positions of *both hands* are computed. This is particularly challenging using an IMU, as small errors compound over time, leading to large positional drift. ArmTrack [33] and MUSE [32] both use the IMUs in a smartwatch for tracking the user's arm movement and demonstrate state-of-the-art drift mitigation methods. RisQ [27] uses the IMU sensor to estimate the position of the wrist to detect smoking and eating behavior.

Compared to existing works, MagX demonstrates comparable wearability and flexibility.Specifically, users can customize the placement of the MagX's tracker and magnet(s) for different use cases, including tracking both hands at the same time with one magnet on each hand. While prior works only require a single point of instrumentation (e.g., smartwatches and Fitbit wristband), they subsequently can only track the hand that wears the device, a fundamental limitation that may severely undermine their usability. Furthermore, these approaches often employ supervised learning methods, which require off-smartwatch compute. MagX's modest compute requirements suggest future on-smartwatch viability.

Vision-based. A popular alternative to IMU approaches is vision-based approach [19, 31, 43], which use cameras to detect fine-grained hand pose and build gesture models upon the location of the fingers/hands. For example, Digits [19] uses an IR camera/laser combination to find the location of the fingers and uses a custom kinematic model to drive interactive applications. While vision approaches are robust against positional drift issues, they present privacy, power, and compute constraints. MagX is not privacy-intrusive and able to achieve NLOS tracking — a fundamental limitation for vision-based tracking schemes.

RF-based. An emerging approach for hand tracking relies on radio frequency (RF). By analyzing the reflected RF signal using radar techniques, movement information can be retrieved. For example, Soli [23] used 60 GHz RF to achieve high-resolution hand pose recognition. However, high-frequency RF signal (e.g., millimeter-wave) can also suffer from NLOS issues, and its power requirements may not be appropriate for continuous battery usage. Conversely, approaches using lower frequencies have significantly less power draw (or are battery-free in the case of RFID [39]) but suffer from significant multipath issues, posing challenges in fine-grained hands tracking applications.

Other tracking modalities. SaveFace [29] proposed a microphone method for detecting face touching events. It leveraged COTS smartphone microphone and radar techniques to achieve the goal. Despite its low-cost feature, this approach requires extensive training and only supports binary classification as it does not track the hands outside certain proximity to the face. FingerIO [25] built an ultrasound radar for tracking 2D finger movement by using a COTS smartphone. However, it tracks finger movement relative to the hands, but not the hand's position relative to the body.

2.2 Magnetic Tracking/positioning

Sensing magnetic induction. One magnetic tracking approach is sensing the current induced on a coil by a magnet. Compared to other magnetic tracking approaches, induction methods have particularly high tracking accuracy and long sensing range. Aura [42] uses electromagnetic induction to achieve fine-grained 3-space tracking of a controller in VR environments. Researchers also [16] simulated electromagnetic induction-based motion tracking by wrapping coils on the human body. Recently, researchers also proposed magnetic induction as a new IoT device tracking schema [34]. However, ultimately, these approaches require an energy-intensive magnetic field generator as a spatial anchor and relatively large induction coil on the object being tracked, making them unsuitable for certain applications or form factors.

Tracking electromagnetic field. Another approach is measuring changes in magnetic fields to localize electromagnets. Finexus [14] uses electromagnets for tracking finger movements in close ranges (e.g., within 12 *cm*). Each electromagnet generates an oscillating magnetic field at specific frequencies, which is then picked up by magnetometers. Electromagnets allow modulation of the magnetic field, allowing richer channel information. However, this approach requires users to wear powered electromagnets, thus reducing wearability and impacting battery-powered applications.

Tracking passive magnet. Most similar to MagX are passive magnet approaches, where magnetometers are used to track passive magnets. Recently, researchers proposed an LM-based method [35] that tracks the position of passive magnets across short distances. However, this approach requires a large array of 16 magnetometers, which may undermine its wearability in the real-world. TRing [44] uses the magnetometer in a ring with a passive magnet in embedded objects for interactive object applications. However, it does not sense the magnet orientation and can only track a single magnet within 5 *cm*. [17] explored magnetic tracking in the driving context. Specifically, it used a commodity smartwatch to sense one passive magnet worn on the other wrist. Instead of tracking the exact position of the magnet, it proposed a machine-learning-based approach to recognize seven pre-defined hand positions based on the magnetometer readings. Furthermore, it focused solely on the recognition of hand position in the driving context. Therefore, its usage scenario and proposed technology are different from ours.

3 ALGORITHM DESIGN OF MAGX

Fig. 2 depicts the system overview of MagX. Specifically, the user needs to wear the magnet(s) and MagX's sensor array (as shown in Fig. 1). The design of our sensor array will be elaborated in

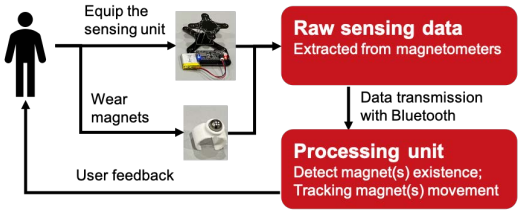

Figure 2: System overview of MagX.

Sec. 4. During operation, the sensor array sends the raw magnetometer data (i.e., 3-axis data from eight sensor elements) to the mobile processing unit. As we will elaborate in Sec. 3.2, MagX first determines the presence of a target magnet(s). This is an important step for achieving robust tracking performance. Then, a LM-based algorithm will be executed for tracking the magnet(s). Note that MagX optimizes the tracking algorithm to enable real-time and light-weight data processing.

3.1 Tracking Algorithm

MagX tracks the movement of magnet(s) by sensing the varying spatial distribution of magnetic field, which can be modeled by using the dipole model [13]. Detailed mathematical modeling of the single-dipole magnet is described by the following formula:

$$\vec{B} = \frac{\mu_0}{4\pi}\left(\frac{3(\vec{m}\cdot\vec{r})\vec{r}}{|\vec{r}|^5} - \frac{\vec{m}}{|\vec{r}|^3}\right) \tag{1}$$

where the $\vec{r}$ is the vector pointing from the magnet to the observation point; $\vec{m}$ is the magnet moment vector.

Hence, to track one magnet, we need to solve for six parameters, i.e., x, y, z, m_x, m_y, m_z, where (x, y, z) and (m_x, m_y, m_z) are $\vec{r}$ and $\vec{m}$, respectively. Since the magnitude of the magnetic moment is a constant, we can describe the magnet moment in a spherical coordinate system.

$$\vec{m} = m\begin{pmatrix} \sin\theta\cos\phi \\ \sin\theta\sin\phi \\ \cos\theta \end{pmatrix} \tag{2}$$

Based on this transaction, the goal of our algorithm is to track six parameters (i.e., x, y, z, m, θ, and ϕ).

To accurately track the magnet, we need to differentiate the targeted magnet's field from the spatially uniform background magnetic field, e.g., the Earth magnetic field. This background magnetic field cannot be ignored, since the magnetic field strength of a dipole degrades at the power of three with respect to the distance [13]. We conduct an experiment study with four N40 grade spherical neodymium magnets with different diameters. Specifically, the corresponding diameters for magnet 1, 2, 3, and 4 are are 20 mm, 15 mm, 10 mm, and 4 mm, respectively. According to our measurement shown in Fig. 3, the magnetic field strength of the strongest magnet (i.e., magnet 1) used in our experiment degrades to the background field strength[1] at approximately 20 *cm*. Thus, to accurately model the system, the magnet field observed on the i-th sensor should be represented as the linear combination of the magnet field generated

[1]The Earth magnetic field ranges from 20 to 60μT [3]

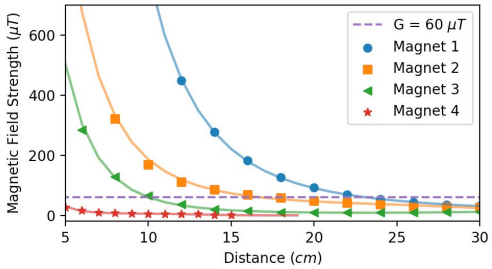

Figure 3: Magnetic field strength of various readily-available magnets across distances

by each magnet and the background magnetic field:

$$\vec{B_i} = G + \sum_{j=1}^{j=M} \frac{\mu_0}{4\pi}\left(\frac{3(\vec{m_j}\cdot\vec{r_{ij}})\vec{r_{ij}}}{|\vec{r_{ij}}|^5} - \frac{\vec{m_j}}{|\vec{r_{ij}}|^3}\right) \tag{3}$$

where $\vec{r_{ij}}$ is the vector pointing from the j^{th} magnet to the i^{th} sensor. In order to track the magnet using the sensor readings in a reliable way, MagX should also interpret the background magnetic field, making it $3+6n$ parameters required in total to track n magnet.

For each sensor, we can establish three equations with respect to three different axes. Noted that it's a combination of nonlinear equations that are hard to find the numerical solution. In order to solve these equations, we use the Levenberg-Marquardt (LM) algorithm [24]. By providing the initial guess and the Jacobian matrix at that point, the LM algorithm can find the local minimum in an iterative fashion.

Considering the environmental noises have a significant impact on the tracking performance, we take two countermeasures: a sliding window filter and a Kalman filter [41]. A sliding window of width 3 is applied to the sensor readings to suppress abnormal high-frequency noises. The Kalman filter is used on the output of the LM algorithm for smoothing the tracking path and providing a feasible guess for the initialization of the next data point.

3.2 The Diminishing Magnets Problem

An algorithm for determining the existence of magnet(s) within the sensing range is necessary, as the magnetic strength of a dipole degrades at the power of three with respect to the distance [13] — a magnet placed at far-field would be too subtle to be sensed by a magnetometer, making it power-consuming and inaccurate to track far-field magnet(s). We defined this issue as the *diminishing magnets problem*. Thus, we would like to trigger the tracking algorithm only if there is at least one magnet within a predetermined sensing range.

Due to the high complexity of the analytical model of the magnetic field, we investigated a data-driven solution. However, conducting a thorough study of the real-world magnetic data is a challenging task, since we could not cover all possible data points in the sensing range. Therefore, a simulation-driven method is proposed. The simulation system, which will be further discussed in Sec. 4.1.2, is used to generate sensor readings under the condition that two magnets are placed at *random* position and orientation. During simulation, the magnet moment and the strength of the earth magnetic field are constant.

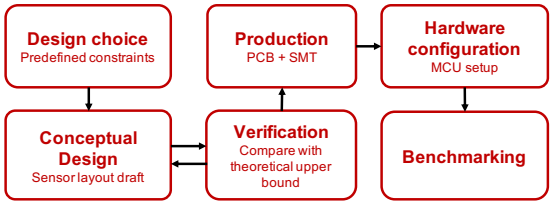

Figure 4: The overview of CAMAD design pipeline

We label the sensor readings into the following two categories: zero vs. one/two magnet(s) within the sensing range. The sensing range is chosen according to the tracking performance (the maximum distance where the tracking error is within 2 *cm*). We simulated 3×10^4 data and labeled them accordingly.

The simulated data is fed into a SVM classifier using the radial basis function (RBF) kernel and parameters $C = 3000$, $\gamma = 1.0 \times 10^{-6}$ to identify the existence of the magnet(s) in the sensing range. Table 1 shows the precision, recall, and F1-score of the SVM classifier on the test set. The average F1-score is above 90%.

	Precision	Recall	F1-score	Support
0	0.98	0.81	0.89	10000
1 or 2	0.91	0.99	0.95	20000

Table 1: SVM classification results to determine the presence of a tracking magnet.

By applying this algorithm, MagX will not invoke the LM algorithm to track the magnet unless the magnet is detected within the sensing ranging. Therefore, MagX can switch between tracking and idling mode to provide an energy-efficient performance.

4 HARDWARE DESIGN OF MAGX

Building the hardware of a novel magnetic sensing array could be a daunting task, as the design-manufacture-debug iteration can be time-consuming and labor-intensive. Our hardware design is guided by the following key design principles:

(1) **Sensing accuracy.** Tracking magnet(s) accurately is the fundamental requirement of our design.
(2) **Interactive range.** MagX should support a sufficient sensing range for real-world hand tracking applications.
(3) **Minimize the energy and manufacturing cost.** A large number of magnetometer sensors and high manufacturing cost would significantly limit the usability of MagX.

We streamline the above design principles and propose a Computer-aided magnetometer array design (CAMAD) pipeline, thus achieving high sensing accuracy with customizable interactive range and minimal costs.

4.1 CAMAD Pipeline Design

4.1.1 Conceptual layout design. Tracking two magnets includes identifying 15 DoFs of information. Since each magnetometer provides information on 3 DoFs, in theory, five magnetometers are needed. To make the system more robust and accurate while limiting power drain, eight magnetometers would be used in our system.

We proposed a two-layer layout for these eight sensors. On one hand, splitting sensors on multiple layers can maximize the distance between each sensor while minimizing the projection of the array on any plane. In other words, this design can make the array smaller without sacrificing the distance between sensors. On the other hand, it would be technically easier and cheaper to produce a PCB board with two layers compared to three or more layers. Besides, a multi-layer PCB uses pin headers to communicate between layers. The number of pin headers increases with more layers, and using too many pin headers may introduce noise to data transmission. To this end, we choose the two-layer layout.

After deciding on a two-layer layout, the distance between the upper and lower layer needs to be determined. This involves balancing between sensor distance, user experience, and market availability. Naturally, the distance between layers should be large so that spatial information gathered by the sensors will be more diverse. However, a large distance between layers might make the device too bulky to wear. Furthermore, the pin headers connecting the upper and lower layer should be commercially available. To this end, the upper-lower layer distance is designed to be 3.2 *cm*.

Based on these premises, we propose the design shown in Fig. 5(b). Sensors on the lower and upper layer are placed on the four vertices of 2 squares. The lower layer square and the upper layer square are staggered so that the diagonal line of the upper square is parallel to the central axis of the lower square. Not only does this design maximize the distance between different sensors, the design can also minimize potential shielding issues caused by large copper PCB boards by hollowing out unused parts of the PCB boards.

To validate that our design can achieve the best accuracy among all sensor layouts designed based on the same constraints (i.e., eight sensors, two-layer layout, the distance between layers being 3.2 cm), we use the following procedures to find one of the optimal layouts in order to compare the performance of our proposed layout with the theoretical upper bound.

4.1.2 Simulation settings. The premise of finding an optimal layout with the aid of a computer is simulating the magnetic field of a magnet and the corresponding measurement. In the simulation process, we use the dipole model and assume there is no interference between two magnets. Therefore, the magnetic field strength collected by the i^{th} sensor can be depicted as the linear combination of the magnet field as modeled in Eq. (3).

We proposed a three-step simulation process: simulating the ideal sensor readings, adding sensor noise, and quantifying sensor readings. First, we compute the theoretical magnetometer readings (i.e., without noises) given the magnet parameters: position, orientation, magnet moment, and the sensor layout. The reading is computed by using Eqs. (1) and (2). The background magnetic field strength in the equation is set to $50\mu T$ by looking up the local Earth magnetic field strength. The second step is to add Gaussian noise according to the datasheet of the magnetometer model. In this paper, we select MLX90393 [4], a popular COTS magnetometer. At the sample rate of 17Hz, the standard deviations of the measurement noises on each axis are $(0.6, 0.6, 1.1)\mu T$ and the least significant bit is $0.15\mu T$. Finally, the sensor reading is quantified according to the sensor resolution (indicated in the datasheet). The simulation result is time-series magnetometer readings corresponding to the magnet's moving trajectory. We implemented the simulation process with NumPy. Sec. 5.2.3 compares our simulation results with

experimental results, validating the simulation (as shown in Fig. 10.

4.1.3 Particle swarm optimization (PSO) Algorithm. The simulation data is used to evaluate the performance of the sensor array. Naturally, our goal is to find the layout that would have the best tracking accuracy. However, finding the optimal layout is an NP-hard problem as the placement combination of magnetic sensors is uncountable. The gradient-based optimization would also fall short as LM algorithm is indifferentiable. The above observations lead us to PSO algorithm [18], a non-gradient optimization method. We elaborate the algorithm for finding the optimal layout as follows. First, we randomly initialize 500 possible layouts (given 8 sensors placed on two parallel planes), each layout is denoted as a particle in the PSO algorithm. Each particle is a 24-dimensional array for representing the 3D positions of 8 magnetometers. Our goal is to find the overall optimal layout from 500 candidates. In each iteration, every particle updates its position and velocity by using the PSO update rule (as shown in Eq. (4)). The objective function is the tracking performance of one moving magnet within a usage-dependent range. For example, in the face touching detection application, the distance between the sensory board (as shown in Fig. 12) and the boundary of the user's face is within 30cm. Then, within the sensing range, we uniformly sample data points to evaluate the layout's tracking performance. After each iteration, each particle updates its best layout and the corresponding objective function value. The global optimal result is also updated. Finally, the algorithm stops at 1000 iterations and the resulting global best solution is used as the optimal layout. The overall pipeline to find the optimal layout is written using NumPy. We implemented the LM algorithm for tracking magnet(s) in C++ with Ceres-solver library.

We define that each particle contains the position information of all n sensors, rendering each particle an array of size $3n$. Based on the constraints in Sec. 4.1.1, we specify that these sensors should be placed on two parallel planes and should be placed within a square on each plane. The distance between the upper and lower plane should be 3.2 cm. At each iteration, each sensor in the particle will update its speed and position according to Eq. (4):

$$\begin{cases} V_i^t = \omega V_i^{t-1} + c_1 r_1 (r_{best(i)}^{t-1} - r_i^{t-1}) + c_2 r_2 (r_{global}^{t-1} - r_i^{t-1}) \\ r_i^t = r_i^{t-1} + V_i^t \end{cases} \tag{4}$$

where ω, c_1 ,and c_2 are hyper-parameters; r_1 and r_2 are random numbers drawn from the uniform distribution between 0 and 1.

However, since the n sensors are interchangeable, the optimal solution may have different expressions and can be misleading. As a result, at each iteration, we sort the sensors based on their coordinates to avoid the duality of the optimal solution.

4.1.4 Objective function. The most intuitive idea to evaluate the performance of the sensor array is to compare the average tracking error of the LM algorithm with a pre-defined route. But this method has two drawbacks: (1) the tracking error will be affected by the random noises; (2) the moving route may not reveal the overall tracking performance of the sensor array. To overcome these drawbacks, we use an objective function based on unscented transformation [37]. The unscented transformation is used to evaluate the effect of applying a nonlinear transformation to a probability distribution. The

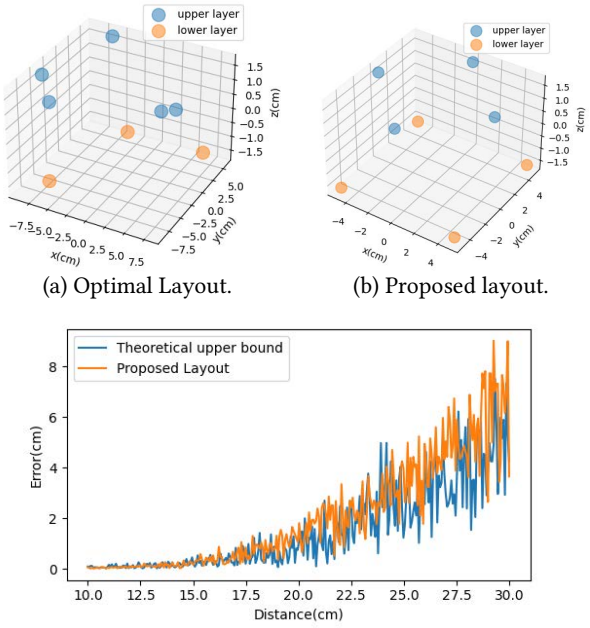

(a) Optimal Layout. (b) Proposed layout.

(c) Simulation Tracking Error.

Figure 5: Comparison of simulated tracking errors for the optimal and proposed sensory array layouts.

key idea is to select some points, denoted as the Σ points, in the original distribution, pass them through the nonlinear function and evaluate the mean and variance of the resulting distribution. The constraints for choosing the Σ are listed in Eq. (5).

$$\begin{aligned} 1 &= \sum_i w_i^m, 1 = \sum_i w_i^c, \mu = \sum_i w_i^m f(\mathcal{X}_i) \\ \Sigma &= \sum_i w_i^c (f(\mathcal{X})_i - \mu)(f(\mathcal{X})_i - \mu)^{\mathsf{T}} \end{aligned} \tag{5}$$

Each Σ point converts to value $\mathcal{Y}$ through the nonlinear transformation. The mean value and variance of the resulting distribution can be calculated using Eq. (5).

$$\mu = \sum_{i=0}^{2n} w_i^m \mathcal{Y}_i, \qquad \Sigma = \sum_{i=0}^{2n} w_i^c (\mathcal{Y}_i - \mu)(\mathcal{Y}_i - \mu)^{\mathsf{T}} \tag{6}$$

Since the LM algorithm is a non-linear function that maps the sensor reading to the magnet position, we use unscented transformation to calculate the uncertainty of the tracking result. The sensor reading is modeled as a normal distribution with ideal sensor reading as mean and measurement noise as variance. By applying the unscented transformation to the sensor reading distribution, we can calculate the mean value and variance of the magnet position. Using the norm of the eigenvalues of the magnet position co-variance matrix, we can measure the uncertainty of the tracking result in a deterministic way.

During the simulation process, we uniformly sample points distributed between 10 *cm* and 30 *cm* from the center of the array. We use the mean value of the tracking uncertainty of these points as the objective function.

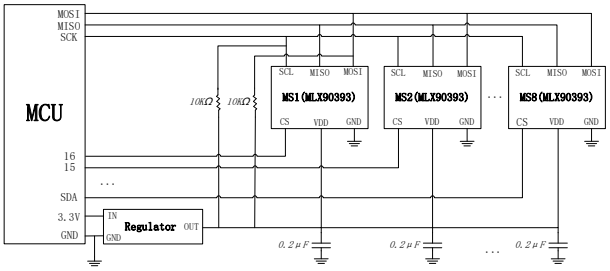

Figure 6: The MagX sensor array circuit schematic.

4.1.5 Simulation result. The resulting layout is listed in Fig. 5(a). Compared to our proposed layout in Sec. 4.1.1, the optimal layout has five instead of four sensors on the upper layer, and the sensors are arranged asymmetrically with two of the five sensors closely allocated. This makes it more challenging to build the optimal layout. The comparison between our proposed layout and the optimal one in Fig. 5(c) shows that the tracking performance of our layout is comparable to the optimal one at varying distance. Thus, by considering both the manufacturing cost and the tracking performance, we conclude that the layout proposed in Sec. 4.1.1 is feasible.

4.2 Hardware Configuration

Based on the layout proposed in Sec. 4.1.1, we manufactured 3 different sensor arrays of size 6×6 cm, 8×8 *cm* and 9.8×9.8 cm. Here $a \times a$ *cm* refers to the size of the square formed by the sensors on the lower layer. The distance between the upper and lower layer is 3.2 cm. The sensor arrays are shown in Fig. 1, and the circuit schematic is shown in Fig. 6.

4.2.1 Magnetometer setting. MLX90393 magnetometers are used in our current system. We choose this specific model as it has a wide dynamic range (i.e., $5 - 50mT$) compared to other commercially available products. A magnetometer with narrower dynamic range may get saturated in our user case with strong magnets placed at near-field.

To minimize the noise and maximize the resolution of the measurement on the premise of smooth user interaction with high frame rate, we tune our MLX90393 chips by setting the following parameters: gain setting (GAIN_SEL), sensor reading resolution (RES), sampling ration (OSR), and digital filter (DIG_FILT) to 7, 0, 3, and 5, respectively.

Gathered magnetic field measurements are sent to an Adafruit Feather nRF52832 before being relayed to the computing unit via Bluetooth Low Energy (BLE) channel.

The Adafruit Feather nRF52832 communicates with the magnetometers via SPI protocol at 2 MHz clock frequency. Compared to I2C protocol, SPI enables faster communication and thus more synchronized reading between multiple magnetometers. Under these configurations, the system can achieve an overall sample rate of 17 Hz, with Z-axis noise lower than 1.1 uT and XY-axis noise lower than 0.6 uT.

4.2.2 Magnetometer calibration. The reading of magnetometers can be easily polluted by hard-/soft-iron effect. Thus, we calibrate the magnetometers against Earth's magnetic field following the standard procedure. We first keep the magnetometers array far away from any magnet in the environment, then gather the reading of the magnetometers while randomly rotating the array. The raw data from the magnetometers have a different scale and bias, as shown in Fig. 7(a). These errors are then removed using the standard calibration algorithm [28]. The sensory array would be ready for tracking when all magnetometers perform uniformly, as shown in Fig. 7(b). Since the intrinsic hard and soft-iron effects of the sensing platform were stable during operation, we only need to calibrate once before conducting a series of experiments/usages.

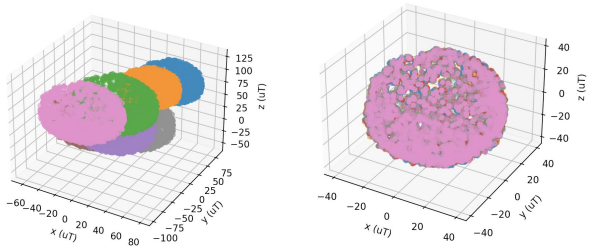

(a) Before calibration. (b) After calibration.

Figure 7: Scatter plot of magnetometer measurements before and after calibration. Each sphere of a distinct color represents the reading of a magnetometer.

5 EVALUATION OF MAGX

5.1 Implementation Details of MagX

In our proposed tracking algorithm, the most time-consuming part is the LM algorithm. We first validate the algorithm by implementing the code using SciPy [38] in Python. The SciPy implementation achieves a frame rate of 20 FPS on a MacBook Pro (15" screen, 2018, Intel i7 CPU 4.0 GHz). In order to improve performance, we implement an optimized LM algorithm in C++ by using the Ceres Solver library [12], a high-performance non-linear solving library. The C++ implementation is wrapped using pybind11 to invoke the C++ implementation within Python, achieving 4000 FPS on the same hardware. This optimization allows MagX to perform all compute on lower power IoT devices, e.g., Raspberry Pi 4B and Zero. For detailed implementation and evaluation, please refer to Sec. 5.3.

5.2 Pilot Study of MagX

5.2.1 A Leap Motion-assisted benchmarking tool. We propose a Leap Motion-assisted benchmarking tool to characterize the position and orientation tracking accuracy of MagX. The Leap Motion controller is a binocular optical tracking module that captures the movements of hands and pen-shaped tools. According to Weichert *et al.* [40], a Leap Motion controller can track pen-shaped tool tips at an accuracy of within 2.5 *mm* (on an average of 1.2 mm), which is an order-of-magnitude lower than the targeted tracking accuracy of our system. Moreover, existing magnetic sensing approaches usually benchmark their systems with high-cost MoCap sets, which can easily cost between \$2k-\$15k [6], a prohibitive hurdle for developing and evaluating novel platforms. In contrast, our prototype system costs less than \$200.

We leveraged this tool tracking ability and designed the pen-shaped tool shown in Fig. 8(a). The pen-shaped tool consists of three parts: a 3D-printed 20cm long cylindrical stick with diameter

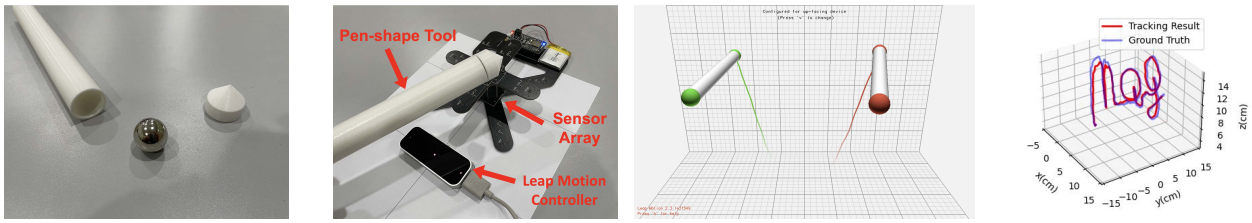

(a) Pen-shaped tool (b) Experimental setting (c) Leap Motion output (d) Tracking traces

Figure 8: Experimental setup of collecting ground truth data. Note that (d) shows the tracking result versus the ground truth when the word "mag" was written in space.

of 24 *mm* and a semi-spherical slot on top, an N40 grade spherical neodymium magnet with diameter of 20 mm, and a 3D-printed cap with a tip. We chose a spherical magnet because its magnetic field flux distribution is close to the dipole model. The magnet was then embedded at the top of the stick and enclosed by the cap, with its north pole pointing towards the tip.

The entire experimental setup is depicted in Fig. 8(b). Before conducting experiments, we calibrated the MagX sensor array according to the procedure in Sec. 4.2.2. During an experiment, Leap Motion's 2.3.1 Python SDK first reported the position and orientation of the tool (Fig. 8(c)). With this information and the dimension of the cap, we can then backtrack the position and orientation of the magnet in the Leap Motion controller's coordinate system. Finally, the position and orientation were translated to the coordinate system of MagX, and was compared with the output of our tracking algorithm for evaluation. Our benchmarking tool allows *free-form* evaluation. Fig. 8(d) illustrates the tracking result vs. the ground truth (collected from Leap Motion) when the word "mag" was written in space.

5.2.2 Position and orientation tracking accuracy. For measuring the position tracking accuracy of MagX, the magnets were moving vertically in the field of view of the Leap Motion controller with a fixed orientation. For measuring the orientation tracking accuracy, angular movement (a zigzag uplifting pattern) was added to the previous moving pattern.

The position and orientation tracking accuracy of one and two magnets tracking are shown in Fig. 9. Each bar consists of 233 data points on average. We define the distance as the Euclidean distance between the centroids of the magnet and sensor array. According to the bar plots, the error grows exponentially with distance. Generally, *accuracy increases as sensor array size increases*, i.e., the 9.8×9.8 layout outperforms other layouts. Some results at close distances might not strictly follow this observation, which is hypothetically due to the fact that our magnet is not a perfect dipole (e.g., due to the imperfect manufacturing). Besides, the process of locating the north pole of a spherical magnet might also introduce error to the ground truth of orientation. *The performance of tracking two magnets is generally lower than that of one magnet due to the doubled unsolved parameters.*

Fig. 9 shows that the average tracking accuracy of the best performing sensor array is 1.7 *cm* (STD: 0.62 cm) and 0.18 rad (STD: 0.06 rad) for 1 magnet, and 2.6 *cm* (STD: 0.46 cm) and 0.54 rad (STD: 0.29 rad) on 2 magnets within 29 *cm* distance. Even the smallest sensor array can achieve an accuracy of 1.8 *cm* (STD: 0.17 cm) and 0.13 rad (STD: 0.02 rad) on 1 magnet, and 2.2 *cm* (STD: 0.27 cm) and 0.26 rad (STD: 0.12 rad) on 2 magnets within 19 cm. These experiment results show that MagX would be sufficient for a wide range of applications, which we will sketch in Sec. 6 as proof of concept applications.

5.2.3 Comparison between simulation and experiment result. In Sec. 3, a simulation tool was used to find the optimal layout of MagX. After gathering the experimental tracking results, we compared them with simulation to validate the CAMAD pipeline.

Fig. 10 shows the comparison between the simulation and experimental results on the 6×6 sensor layout. At short distance, tracking accuracy of the simulation is shown to be better than that of the experiment. We conjecture that this is because the simulation assumes the magnet to follow the ideal dipole model, while the magnetic field flux may slightly deviate from the dipole model in the real-world. As distance increases, simulation and experiment results were observed to match up, confirming our conjecture: the magnetic field around any magnet looks increasingly like the field of a dipole as the distance from the magnet increases. Thus, we conclude that our simulation results are valid, especially when distance is greater than or equal to 20 cm.

5.2.4 Comparison between different magnet sizes. Apart from the size of the sensor array, the size of magnet will also affect tracking accuracy, since different magnets' sizes may shape the morphological feature of the magnetic field.

Based on the result from the previous benchmarking section which uses N40 grade spherical neodymium magnets with 20 *mm* diameter, we further tested the tracking performance of magnets of the same material but with 15 *mm* and 10 *mm* diameter on the 6×6 layout. The comparison results are shown in Fig. 11. As illustrated in the figure, tracking performances of magnets of different sizes are comparable at a close distance. When the distance increases, the larger the magnet, the higher the tracking accuracy.

5.3 Overheads of MagX

We conduct a thorough overhead analysis of MagX's sensing array and computing unit. In our experiment, we profiled the energy drain of our sensor array and computing unit by using a power meter (with measurement accuracy of 0.001 W). For the CPU usage, we used htop command line tool.

The experimental results showed an average of 0.22 W power drain on MagX sensor array during operation at full sampling speed. Therefore, with our small battery pack (lithium Ion polymer battery of 3.7 V, 500 mAh), akin to smartwatch's battery capacity, MagX's

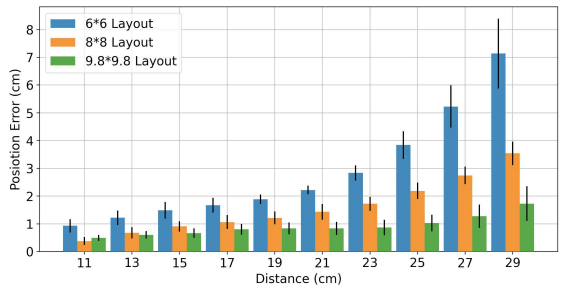

(a) Position error of tracking **one** magnet

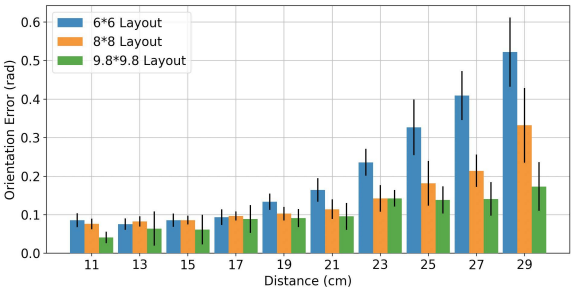

(b) Orientation error of tracking **one** magnet

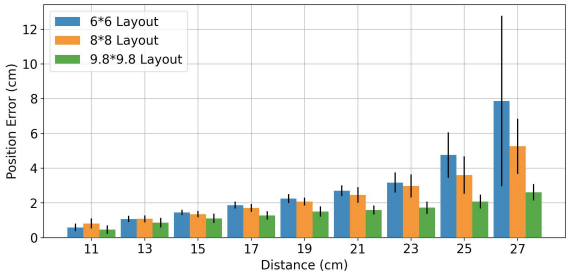

(c) Position error of tracking **two** magnet

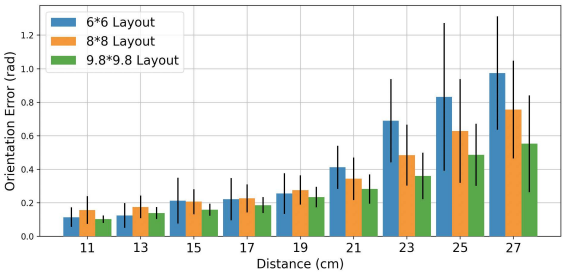

(d) Orientation error of tracking **two** magnets

Figure 9: Position and orientation tracking performance of one and two magnets on three different sizes arrays.

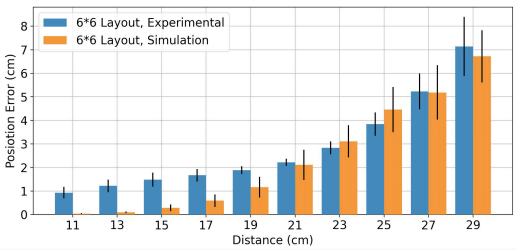

Figure 10: Comparison between simulation and experiment result on 6×6 layout.

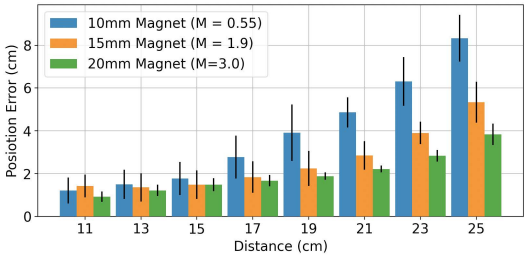

Figure 11: Comparison of the tracking result of three different magnets on 6×6 layout.

sensing array can last about 8 hours — sufficient battery life for various real-world applications. One can easily boost MagX's battery life with a larger battery pack without compromising its wearability. Future implementations can explore dynamic sampling rates and employ hardware interrupts to wake/sleep the array for further power consumption improvement.

Additionally, we implement MagX using a Raspberry Pi 4B with 8G of memory to analyze its performance on mobile devices. To push it to the limit, we further test the system on a emulated environment of Raspberry Pi Zero, a tiny low-power hardware. Considering that the Raspberry Pi Zero is equipped with a 1 GHz single-core CPU, while a Raspberry Pi 4B is equipped with a 1.5 GHz quad-core CPU, limiting the CPU power to 17% is reasonable for the emulation. These two setups are compared in Table 2. Even with 13.1% of the CPU usage, our algorithm can still maintain 42% of the tracking speed, making MagX feasible to be implemented on COTS low power-consumption IoT devices such as *smartwatch*. Note that, the ultra-low power drain of 0.159 W enables 16-hour usage for the computation node on a 500 mAh battery. For further decreased compute power requirements, future implementations can explore on-microcontroller or hardware-accelerated implementations.

CPU Quota	CPU Usage	Average FPS	Power Drain
100%	181.21%	1213.89	0.643w
17%	23.79%	514.23	0.159w

Table 2: Comparison between a fully and a 17% (Pi Zero emulation) powered Raspberry Pi 4B.

6 USE CASES OF MAGX

We outline three applications to showcase the versatility of MagX: face-touch detection, controller-free AR interaction, and endocapsule tracking. For each use case, we introduce the form factor specifications (i.e., sensor array size, magnet size, placement), followed by experimental results.

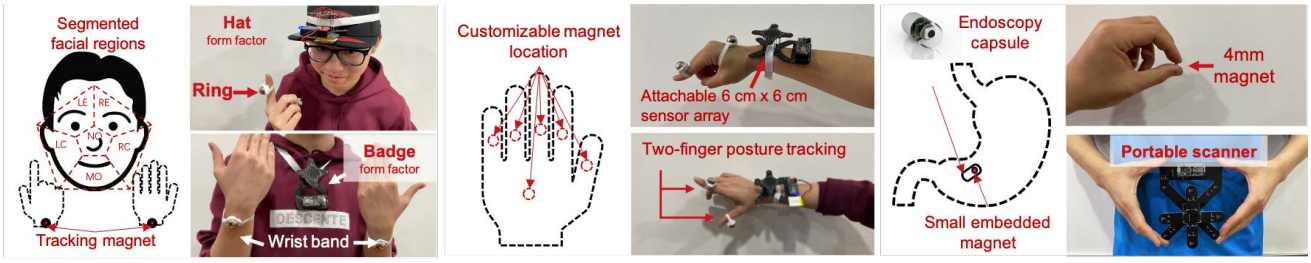

(a) Face touching tracking (b) AR interaction (c) Endoscopy tracking

Figure 12: Three use cases of MagX. (a) tracking face touching behavior with passive magnets on both hands; and (c) controller-free free form AR interaction; (d) tracking endocapsule movement.

6.1 Face-touch tracking

People subconsciously touch their face (e.g., eyes, ears, nose, and mouth) 23 times/hour [20] on average, letting bacteria and viruses enter the body through mucous membranes, leading to staph and other severe respiratory infections (e.g., COVID-19). Therefore, detecting and reducing face-touch events could significantly limit the spread of diseases.

MagX can help enable two novel form factors, i.e., the cap and badge (as shown in Fig. 12). For the cap form factor, the user will be wearing a cap with the sensor array placed on the brim and two magnet rings on two index fingers. Since the magnets are directly attached to the fingers, their positions can serve as good approximations of fingertip positions. For the badge form factor, sensor array and magnets should be placed at the user's chest and wrists, respectively. To find the fingertip positions, the magnets are places on the user's wrists with its north pole pointing towards where relaxed fingertips naturally lie. In this way, the positions of index fingertips can be approximated with magnets' position and orientation together with the length of a relaxed hand.

In both form factors, the 6×6 sensor array and 20 *mm* magnets are used. Both form factors assume that an unconscious face touching event only involves one hand. Thus, the one-magnet tracking algorithm is adopted.

Users' wearing of MagX will not be interfered with by each others' magnets. The magnetic field strength degrades quickly as the magnet–sensor distance increases. Under the current settings, i.e., neodymium magnet, MLX90393 magnetometer, and the sensor layout, the sensor readings are overwhelmed by the sensor noise beyond 40*cm*. According to the four zones of inter-person distance (based on the study of proxemics [22]), the intimate personal range is up to 18 inches (45cm) — MagX's sensing range is within the intimate personal zone. Hence, MagX is robust to the interference from the magnets worn by other users.

Compared to prior work on face-touch detection (e.g., using the headphone speaker and microphone on a smartphone), MagX offers three unique advantages:

- **Fine-grained.** MagX can detect face touching at centimeter-level accuracy. This feature can reliably profile the user's face touching behavior, thus enabling new applications. For example, by recognizing the number of eye-rubbing events, MagX can suggest the user visit an eye clinic for eye drops prescriptions.
- **Training-free.** Thanks to the high tracking accuracy, MagX can detect the touched region directly from the derived geometric data, thus achieving a training-free usage modality. The user only needs to provide one-time information of his/her face geometry. We will elaborate an exemplary process in this section.
- **Highly usable.** Compared to the predominant smartwatch-based method, MagX can achieve *two-hand tracking*, allowing seamless face-touch detection.

For the face geometry information, one can use the standard human face geometry measurement or measurement gathered from their own faces. To do this, users will be asked to put their fingers on different regions of their face (i.e., left eye, right eye, nose, mouth, left cheek, and right cheek) and their jaw, left ear, right ear for a short period to collect data. Here, LC, LE, M, N, RC, RE, and No in Fig .13 represents left cheek, left eye, mouth, nose, right cheek, right eye, and no touch, respectively. The tracking results of nose, jaw, left ear, right ear data are used to define the boundary of one's face, while the rest of the data are used to pinpoint each part of their faces. After characterizing their faces, users can start using MagX to track their fingers. Alg. 1 summarizes the detection algorithm.

6.1.1 Experiments. Figs. 13 (a) and (c) show the tracking trajectory of the cap and badge form factors, respectively. The classification results are shown in Figs. 13 (b) and (d). Specifically, the cap form factor shows steady classification performance for all face areas with an average accuracy of 92%. Compared to the cap form factor, the badge has higher wearability by sacrificing certain accuracy. There are two reasons for this: (1) the sensor array is not fixed relative to the user's face; (2) the varying hand posture (e.g., bending the finger) may introduce error when deriving the user's fingertip position based on the wrist position and orientation.

6.2 Controller-free AR Interaction

MagX helps enhance seamless hand-based AR interaction by enabling two essential features: NLOS-resilience and controller-free. These features help several applications, e.g., hands-based interaction under poor lighting conditions.

Users can put the 6×6 MagX on their wrists (shown in Fig. 12(b)), with two 15 *mm* magnets worn in as rings. The two-magnet tracking algorithm constantly tracks the position and orientation of the two magnets. We built a lightweight hand-pose kinematic model (as shown in Fig. 14), which utilizes the position and orientation of

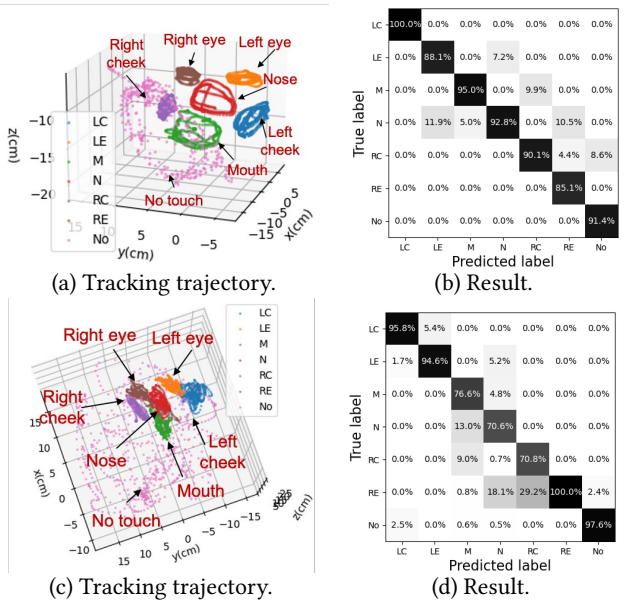

(a) Tracking trajectory. (b) Result.

(c) Tracking trajectory. (d) Result.

Figure 13: The experimental results of face touching. The first and second rows show the performance of the cap and badge form factors, respectively.

Algorithm 1 Algorithm for Face touching detection

```
Inputs:
    Sensor layout, Sensor readings
// Check the magnet existence using SVM
if exist_magnet(readings) = 0 then
    class ← No touch
else
    // Tracking the magnet
    [position, orientation] = LM(reading,layout)
    // Compare the tracking position with face boundary
    if position ∈ boundary then
        // classify the finger position using KNN
        class ← KNN(position)
    else
        class ← No touch
    end if
end if
```

the two magnets to reconstruct poses of fingers that are equipped with the magnets. Note that users can customize the placement of magnets to support different usage scenarios.

Existing AR and finger-tracking solutions utilize gloves equipped with embedded optic sensor (e.g., Nintendo power glove [15]), IMUs [30], and flex sensors. Even though they can track more DoFs of hands than MagX, our system consumes less power and can thus have longer battery life. Furthermore, MagX is less bulky — it only requires the user to wear two magnetic rings, plus a lightweight sensor platform on its wrist. There is no need to cover the entire hands with gloves.

6.2.1 Experiments. We explored four popular hand postures shown in Fig. 14, i.e., neutral, click, finger heart, and stop. By placing the

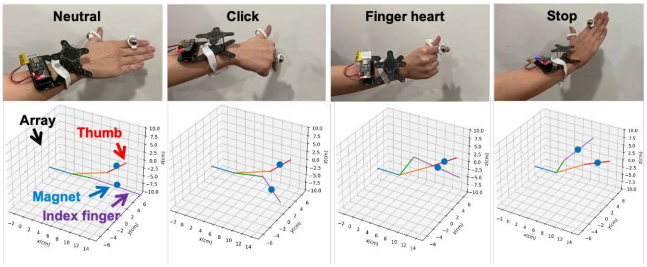

Figure 14: MagX for controller-free AR interaction.

sensor array on the user's wrist, MagX can track the magnets on the user's index finger and thumb. Each hand posture's resulting position and orientation are fed into SVM using RBF kernel with parameter $C = 100$ and $\gamma = 0.001$. Evaluation results are presented in Table 3, with an overall accuracy of >98%. The highly reliable performance of MagX demonstrates the potential for supporting more complicated hand postures.

	Precision	recall	F1-score	Support
Neutral	0.95	1.00	0.98	271
Click	1.00	1.00	1.00	247
Finger heart	1.00	1.00	1.00	302
Stop	1.00	1.00	1.00	253
None	1.00	0.94	0.97	269

Table 3: Evaluation of hand posture classification.

6.3 Endocapsule Tracking

Capsule endoscopy is an emerging medical tool for detecting early-stage intestine tumour with an embedded camera. Patients would be instructed to swallow the capsule for collection of their image data — after the patient swallows the capsule, the doctor can only to access the capsule after its excretion. As shown in [7], the capsule could be stuck in the patient's digestive tracts (e.g., small intestines), causing an urgent surgery. Unlike previous applications, which require "strong" magnets, the endocapsule tracker needs to track an ultra-small magnet because of the endocapsule's compact size, leading to a unique challenge for endocapsule tracking.

To overcome the above challenge, we propose a localization process similar to medical ultrasound testing [26]. After removing all magnetic devices, the user is instructed to place the 9.8×9.8 MagX array on the top of his/her abdomen area (e.g., as shown in Fig. 12(c)). If MagX senses the embedded magnet's position, i.e., the system reports a clear dot measurement with a slight deviation, the endocapsule's position can be presented as $< x', y', z' >$ in the sensor array's coordinate system. Suppose the endocapsule is not within the tracking scope of MagX, i.e., the system reports a null or noisy measurement, the user should adjust MagX sensor's placement and examine the new measurement result. Combining the sensor array's placement and tracking result, one can derive the endocapsule's location in his/her body. To further enhance the accuracy, the system would suggest the user perform multiple measurements at different placement on his/her abdomen.

Compared to existing endocapsule tracking solutions, e.g., X-ray machines, CT machines, and ultrasonography systems [36], MagX is affordable, portable, and lightweight. Therefore, with a tiny (i.e.,

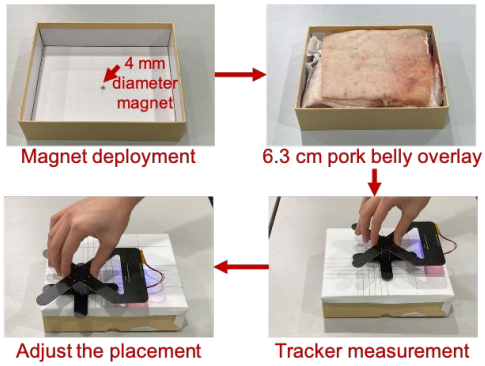

(a) The measurement process.

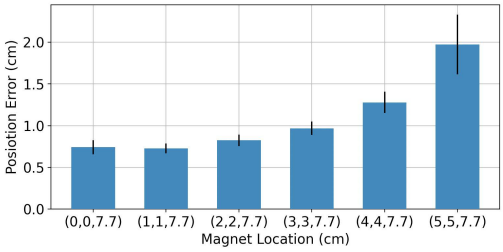

(b) Experiment result.

Figure 15: The experimental result of endocapsule tracking.

4mm in diameter, as shown in Fig. 15) magnet embedded in the capsule, MagX allows for *in-home self-monitoring* of the endocapsule's location and orientation, whereas current approaches are cost-prohibitive and unsuitable for in-home self-care.

6.3.1 Experimental Results. To gain a statistical understanding of MagX's performance, we conducted a real-world experiment for endocapsule tracking. We fixed the small magnet at the bottom of a box then laid a pork belly (with a thickness of 6.3 *cm*, skin on) to cover the magnet. Note that the small magnet's diameter is only 4 *mm* — a feasible size for most existing endocapsules, of which the common dimension is 11 *mm* in diameter and 26 *mm* in length [5]. This ex-vivo setting emulates the patient's usage of MagX as we previously discussed. The numerical results we measured support our findings in Sec. 4. That is, as the Euclidean distance increases, the performance decreases exponentially. Specifically, for (0,0,7.7), (1,1,7.7), (2,2,7.7), (3,3,7.7), (4,4,7.7), and (5,5,7.7) placements, MagX achieves the averaged accuracy of 7.4 *mm* (STD: 0.8 *mm*), 7.3 *mm* (STD: 0.5 *mm*), 8.2 *mm* (STD: 0.5 *mm*), 9.7 *mm* (0.8 *mm*), 12.8 *mm* (1.3 *mm*), and 19.7 *mm* (3.6 *mm*), respectively. Note that the last array placement has a Euclidean distance of 10.45 *cm*, which would be a sufficient scanner-magnet distance.

7 DISCUSSION

7.1 Limitation

Number of magnets. The current version of MagX can track two passive magnets. Tracking multiple magnets requires three DoFs and six DoFs for the background magnetic field and each magnet, respectively. Since each magnetometer provides information on three DoFs, theoretically $2n+1$ magnetometers are needed for tracking n magnets. In practice, for robust tracking, more magnetometers are needed. Our current system can reliably track up to two magnets. Note that, tracking two magnets is sufficient for addressing several crucial hand-tracking problems, e.g., tracking two fingers for the controller-free AR interaction (as discussed in 6.2).

Size of the sensory array. Our current system still takes up a space of $6cm \times 6cm \times 3.2cm$. Despite its compact design, the size is larger than commodity smartwatches. The size of current MagX's form factor is supported by our experimental study. As shown in Fig. 9, to achieve the targeted sensing accuracy (error less than $2cm$ at $20cm$ distance), the sensor array can be no smaller than our current design. By analyzing the tracking performance of sensor arrays of different sizes, we make a trade-off between the array size and accuracy, i.e., a larger array usually yields a higher tracking performance. That is, by determining the accuracy requirement of the application, one can adjust and re-design the sensor array by following the design pipeline (as shown in Sec. 4) of MagX.

7.2 Safety of Passive Magnets

Strong magnetic fields may have adverse health effects. According to the ACGIH, 60 mT is acceptable for routine whole-body exposure and 600 mT for exposure to the extremities[8]. More conservative is the WHO's recent study [1], which recommended the maximum whole-body exposure to magnetic flux density be limited to 2 T and 40 mT for static magnetic field strength. According to our measurement, the strongest magnet used in MagX has a magnetic field strength less than 10 mT at 1 cm, which is safe for daily usage and significantly below both recommendations. Recent concerns regarding the magnets used in iPhones has highlighted concerns regarding patients with cardiac implants [11]. For this population, safe magnetic strength is less than 0.5 mT [2]) and we recommend users consult with their physician.

8 CONCLUSION

This paper presents MagX, a fully wearable and untethered magnetic tracking system with passive magnets. To facilitate the rapid development of novel magnetometer array designs, we proposed a hardware design pipeline, CAMAD, which can validate sensor arrangements and propose optimal sensor layout given a set of parameters, such as distance and magnet strength. We used this tool to optimize the final sensor arrangements of MagX to minimize magnetic strength requirements and maximize effective tracking distance while still maintaining a wearable form factor. We then demonstrate that MagX is a highly wearable, reliable, and energy-efficient tool through three exemplar real-world applications: face touching detection, controller-free AR interaction, and endocapsule tracking. These three examples demonstrate the versatility of MagX as a robust positional tracking method. We hope these results inspire further adoption and exploration of magnetic sensing.

ACKNOWLEDGEMENTS

We thank the anonymous reviewers and shepherd for their feedback. The work reported in this paper is supported in part by National Key R&D Program of China 2018AAA0101202, NSFC (61960206002, 61822206, 62020106005, 61829201, and 42050105). It is also supported in part by the NSF under Grant No. 2034626. Dongyao Chen and Xinbing Wang are corresponding authors.

REFERENCES

[1] 2006. Electromagnetic fields and public health. https://www.who.int/peh-emf/publications/facts/fs299/en/. (2006).

[2] 2011. Neodymium Magnets and Pacemaker Safety. https://www.kjmagnetics.com/blog.asp?p=pacemaker-safety#:~:text=What%20field%20strength%20is%20OK,a%20pacemaker%20will%20operate%20properly.&text=We%20also%20contacted%20Medtronic%2C%20another,limit%20for%20DC%20magnetic%20fields.. (2011).

[3] 2014. Measuring Earth's Magnetism. https://earthobservatory.nasa.gov/images/84266/measuring-earths-magnetism. (2014).

[4] 2017. Melexis: MLX90393 Triaxis® Magnetic Node. https://www.melexis.com/-/media/files/documents/datasheets/mlx90393-datasheet-melexis.pdf. (2017).

[5] 2019a. Capsule Endoscopy. https://www.asge.org/home/about-asge/newsroom/media-backgrounders-detail/wireless-capsule-endoscopy#:~:text=The%20capsule%2C%20which%20is%20swallowed,%2C%20transmitter%2C%20and%20an%20antenna.. (2019).

[6] 2019. High Quality Mocap for a Fraction of the Cost. https://nofilmschool.com/rokoko-review-high-quality-mocap-fraction-cost#:~:text=The%20Rokoko%20Smartsuit%20fills%20an,usually%20cost%20upwards%20of%20%2415%2C000.. (2019).

[7] 2019b. Mayo Clinic: Capsule endoscopy. https://www.mayoclinic.org/tests-procedures/capsule-endoscopy/about/pac-20393366. (2019).

[8] 2020. ACGIH threshold limit values for continuous exposure to static magnetic fields. https://blink.ucsd.edu/safety/radiation/magnet/limits.html. (2020).

[9] 2020. Immutouch wristband buzzes to stop you touching your face. https://techcrunch.com/2020/03/09/dont-immutouch/. (2020).

[10] 2020. JALAPENO! Stop touching your face. Stop smearing your makeup. http://www.jalapenoapp.com/index.html. (2020).

[11] 2021. Henry Ford Cardiologists Find Apple iPhone 12 Magnet Deactivates Implantable Cardiac Devices. https://www.henryford.com/news/2021/02/iphone-12-deactivates-defibrillato. (2021).

[12] Sameer Agarwal, Keir Mierle, and Others. 2020. Ceres Solver. http://ceres-solver.org. (2020).

[13] Jean G. Van Bladel. 2007. *Electromagnetic Fields* (2 ed.). Wiley-IEEE Press.

[14] Ke-Yu Chen, Shwetak N. Patel, and Sean Keller. 2016. Finexus: Tracking Precise Motions of Multiple Fingertips Using Magnetic Sensing. In *Proceedings of the 2016 CHI Conference on Human Factors in Computing Systems*. Association for Computing Machinery, New York, NY, USA, 1504–1514. https://doi.org/10.1145/2858036.2858125

[15] Dana L. Gardner. 1989. The Power Glove. *Design News* (1989). https://www.microsoft.com/buxtoncollection/a/pdf/powerglove%20design%20news%20%20article.pdf?from=http%3A%2F%2Fresearch.microsoft.com%2Fen-us%2Fum%2Fpeople%2Fbibuxton%2Fbuxtoncollection%2Fa%2Fpdf%2Fpowerglove%2520design%2520news%2520%2520article.pdf

[16] Negar Golestani and Mahta Moghaddam. 2020. Human activity recognition using magnetic induction-based motion signals and deep recurrent neural networks. *Nature communications* 11, 1 (2020), 1–11.

[17] Hua Huang, Hongkai Chen, and Shan Lin. 2019. MagTrack: Enabling Safe Driving Monitoring with Wearable Magnetics. In *Proceedings of the 17th Annual International Conference on Mobile Systems, Applications, and Services (MobiSys '19)*. Association for Computing Machinery, New York, NY, USA, 326–339. DOI: http://dx.doi.org/10.1145/3307334.3326107

[18] J. Kennedy and R. Eberhart. 1995. Particle swarm optimization. In *Proceedings of ICNN'95 - International Conference on Neural Networks*, Vol. 4. 1942–1948 vol.4. DOI: http://dx.doi.org/10.1109/ICNN.1995.488968

[19] David Kim, Otmar Hilliges, Shahram Izadi, Alex D. Butler, Jiawen Chen, Iason Oikonomidis, and Patrick Olivier. 2012. Digits: Freehand 3D Interactions Anywhere Using a Wrist-Worn Gloveless Sensor. In *Proceedings of the 25th Annual ACM Symposium on User Interface Software and Technology (UIST '12)*. Association for Computing Machinery, New York, NY, USA, 167–176. DOI: http://dx.doi.org/10.1145/2380116.2380139

[20] Yen Lee Angela Kwok, Jan Gralton, and Mary-Louise McLaws. 2015. Face touching: A frequent habit that has implications for hand hygiene. *American Journal of Infection Control* 43, 2 (2015), 112 – 114. DOI: http://dx.doi.org/https://doi.org/10.1016/j.ajic.2014.10.015

[21] Gierad Laput and Chris Harrison. 2019. Sensing Fine-Grained Hand Activity with Smartwatches. In *Proceedings of the 2019 CHI Conference on Human Factors in Computing Systems (CHI '19)*. Association for Computing Machinery, New York, NY, USA, Article Paper 338, 13 pages. DOI: http://dx.doi.org/10.1145/3290605.3300568

[22] John E. Lewis. 1998. 10.04 - Cross-cultural Clinical Interventions. In *Comprehensive Clinical Psychology*, Alan S. Bellack and Michel Hersen (Eds.). Pergamon, Oxford, 93–125. DOI: http://dx.doi.org/https://doi.org/10.1016/B0080-4270(73)00106-1

[23] Jaime Lien, Nicholas Gillian, M. Emre Karagozler, Patrick Amihood, Carsten Schwesig, Erik Olson, Hakim Raja, and Ivan Poupyrev. 2016. Soli: Ubiquitous Gesture Sensing with Millimeter Wave Radar. *ACM Trans. Graph.* 35, 4, Article 142 (July 2016), 19 pages. DOI: http://dx.doi.org/10.1145/2897824.2925953

[24] J J More. 1977. Levenberg–Marquardt algorithm: implementation and theory. (1 1977). https://www.osti.gov/biblio/7256021

[25] Rajalakshmi Nandakumar, Vikram Iyer, Desney Tan, and Shyamnath Gollakota. 2016. FingerIO: Using Active Sonar for Fine-Grained Finger Tracking. In *Proceedings of the 2016 CHI Conference on Human Factors in Computing Systems (CHI '16)*. Association for Computing Machinery, New York, NY, USA, 1515–1525. DOI: http://dx.doi.org/10.1145/2858036.2858580

[26] Philip ES Palmer. 1995. *Manual of diagnostic ultrasound*. World Health Organization.

[27] Abhinav Parate, Meng-Chieh Chiu, Chaniel Chadowitz, Deepak Ganesan, and Evangelos Kalogerakis. 2014. RisQ: Recognizing Smoking Gestures with Inertial Sensors on a Wristband. In *Proceedings of the 12th Annual International Conference on Mobile Systems, Applications, and Services (MobiSys '14)*. Association for Computing Machinery, New York, NY, USA, 149–161. DOI: http://dx.doi.org/10.1145/2594368.2594379

[28] Timo Pylvänäinen. 2008. Automatic and adaptive calibration of 3D field sensors. *Applied Mathematical Modelling* 32, 4 (2008), 575–587. DOI: http://dx.doi.org/10.1016/j.apm.2007.02.004

[29] Camilo Rojas, Niels Poulsen, Mileva Van Tuyl, Daniel Vargas, Zipporah Cohen, Pattie Maes Joseph A. Paradiso, Kevin M Esvelt, and Fadel Adib. 2021. A Scalable Solution for Signaling Face Touches to Reduce the Spread of Surface-based Pathogens. In *Proceedings of the 2021 ACM International Joint Conference on Pervasive and Ubiquitous Computing (UbiComp '21)*. ACM, New York, NY, USA.

[30] Christina Salchow-HÃ¶mmen, Leonie Callies, Daniel Laidig, Markus Valtin, Thomas Schauer, and Thomas Seel. 2019. A Tangible Solution for Hand Motion Tracking in Clinical Applications. *Sensors* 19, 1 (2019). DOI: http://dx.doi.org/10.3390/s19010208

[31] Toby Sharp, Cem Keskin, Duncan Robertson, Jonathan Taylor, Jamie Shotton, David Kim, Christoph Rhemann, Ido Leichter, Alon Vinnikov, Yichen Wei, Daniel Freedman, Pushmeet Kohli, Eyal Krupka, Andrew Fitzgibbon, and Shahram Izadi. 2015. Accurate, Robust, and Flexible Real-Time Hand Tracking. In *Proceedings of the 33rd Annual ACM Conference on Human Factors in Computing Systems (CHI '15)*. Association for Computing Machinery, New York, NY, USA, 3633–3642. DOI: http://dx.doi.org/10.1145/2702123.2702179

[32] Sheng Shen, Mahanth Gowda, and Romit Roy Choudhury. 2018. Closing the Gaps in Inertial Motion Tracking. In *Proceedings of the 24th Annual International Conference on Mobile Computing and Networking (MobiCom '18)*. Association for Computing Machinery, New York, NY, USA, 429–444. DOI: http://dx.doi.org/10.1145/3241539.3241582

[33] Sheng Shen, He Wang, and Romit Roy Choudhury. 2016. I Am a Smartwatch and I Can Track My User's Arm. In *Proceedings of the 14th Annual International Conference on Mobile Systems, Applications, and Services (MobiSys '16)*. Association for Computing Machinery, New York, NY, USA, 85–96. DOI: http://dx.doi.org/10.1145/2906388.2906407

[34] R. Shirai, Y. Itoh, and M. Hashimoto. 2021. Make it Trackable: An Instant Magnetic Tracking System With Coil-Free Tiny Trackers. *IEEE Access* 9 (2021), 26616–26632. DOI: http://dx.doi.org/10.1109/ACCESS.2021.3057906

[35] C. R. Taylor, H. G. Abramson, and H. M. Herr. 2019. Low-Latency Tracking of Multiple Permanent Magnets. *IEEE Sensors Journal* 19, 23 (2019), 11458–11468. DOI: http://dx.doi.org/10.1109/JSEN.2019.2936766

[36] Ilknur Umay, Barış Fidan, and Billur Barshan. 2017. Localization and tracking of implantable biomedical sensors. *Sensors* 17, 3 (2017), 583.

[37] Rudolph Van Der Merwe, Arnaud Doucet, Nando De Freitas, and Eric Wan. 2001. The unscented particle filter. *Advances in Neural Information Processing Systems* (2001).

[38] Pauli Virtanen and et al. 2020. SciPy 1.0: Fundamental Algorithms for Scientific Computing in Python. *Nature Methods* 17 (2020), 261–272. DOI: http://dx.doi.org/10.1038/s41592-019-0686-2

[39] Jue Wang, Deepak Vasisht, and Dina Katabi. 2014. RF-IDraw: Virtual Touch Screen in the Air Using RF Signals. *SIGCOMM Comput. Commun. Rev.* 44, 4 (Aug. 2014), 235–246. DOI: http://dx.doi.org/10.1145/2740070.2626330

[40] Frank Weichert, Daniel Bachmann, Bartholomäus Rudak, and Denis Fisseler. 2013. Analysis of the accuracy and robustness of the Leap Motion Controller. *Sensors (Switzerland)* 13, 5 (2013), 6380–6393. DOI: http://dx.doi.org/10.3390/s130506380

[41] Greg Welch, Gary Bishop, and others. 1995. An introduction to the Kalman filter. (1995).

[42] Eric Whitmire, Farshid Salemi Parizi, and Shwetak Patel. 2019. Aura: Inside-out Electromagnetic Controller Tracking. In *Proceedings of the 17th Annual International Conference on Mobile Systems, Applications, and Services (MobiSys '19)*. Association for Computing Machinery, New York, NY, USA, 300–312. DOI: http://dx.doi.org/10.1145/3307334.3326090

[43] Hui-Shyong Yeo, Byung-Gook Lee, and Hyotaek Lim. 2015. Hand Tracking and Gesture Recognition System for Human-Computer Interaction Using Low-Cost Hardware. *Multimedia Tools Appl.* 74, 8 (April 2015), 2687–2715. DOI: http://dx.doi.org/10.1007/s11042-013-1501-1

[44] Sang Ho Yoon, Yunbo Zhang, Ke Huo, and Karthik Ramani. 2016. TRing: Instant and Customizable Interactions with Objects Using an Embedded Magnet and a

Finger-Worn Device. In *Proceedings of the 29th Annual Symposium on User Interface Software and Technology (UIST '16)*. Association for Computing Machinery, New York, NY, USA, 169–181. DOI: http://dx.doi.org/10.1145/2984511.2984529